AGU100 ADVANCING EARTH AND SPACE SCIENCE

JGR Space Physics

RESEARCH ARTICLE
10.1029/2019JA027459

Key Points:
- A rigorous probability model for meteor detection is developed
- Detection of meteors in the presence of strong equatorial electrojets allows unbiased study of meteor characteristics
- Many meteors are detected in the second sidelobe and beyond and enter the radar beam with a large arrival angle

Correspondence to:
Q. Zhou,
zhouq@miamioh.edu

Citation:
Li, Y., Zhou, Q., Scott, M., & Milla, M. (2020). A Study on Meteor Head Echo Using a Probabilistic Detection Model at Jicamarca. *Journal of Geophysical Research: Space Physics*, *125*, e2019JA027459. https://doi.org/10.1029/2019JA027459

Received 27 SEP 2019
Accepted 22 DEC 2019
Accepted article online 12 JAN 2020

A Study on Meteor Head Echo Using a Probabilistic Detection Model at Jicamarca

Yanlin Li[1], Qihou Zhou[1], Mark Scott[1], and Marco Milla[2]

[1]Electrical and Computer Engineering Department, Miami University, Oxford, OH, USA, [2]Radio Observatorio de Jicamarca, Instituto Geofísico del Perú, Lima, Perú

Abstract A coded long pulse is applied to the Jicamarca 50 MHz high power large aperture radar to study meteor head echoes. We develop a probabilistic detection model, which finds 25% more meteors than the commonly used signal-to-noise threshold method. The long code and the probabilistic approach allow us to detect over 180 meteors per minute during the dawn hours, which is several times higher than reported previously. The typical mass of the meteoroids is estimated to be about 10^{-9} kg, slightly smaller than other sensitive very-high-frequency and ultrahigh-frequency high power large aperture radars except the Arecibo radar. The high sensitivity allows us to observe numerous meteors in the presence of the strongest equatorial electrojet. We report and discuss the characteristics of meteor flux rate, ablation height, and velocity with a constant noise power for the first time for the Jicamarca radar. The highest average detection height is found to be near 2 a.m., instead of near 6 a.m. when the largest average velocity is observed. This is likely due to the combination of the relative large atmospheric velocity and the substantial atmospheric entry angles around 2 a.m. The observed characteristics suggest that many meteors are detected 8° off zenith despite that the full beam width is only 2.4°.

1. Introduction

High power large aperture radars (HPLARs) have been extensively used for meteor studies since the 1990s (Chapin & Kudeki, 1994; Pellinen-Wannberg & Wannberg, 1994; Zhou et al., 1995). HPLARs at very-high-frequency (VHF) range (<30–300 MHz) typically see both head echoes and spread trail echoes when the radar is pointing perpendicular to the B-field while ultrahigh-frequency radar (0.3–3 GHz) can only observe head echoes (Zhou et al., 2001). The combination of the operating frequency, transmitter power and larger aperture, and pointing direction allows the Jicamarca 50 MHz to observe a large number of head echoes and the range spread trail echoes (RSTE). Chapin and Kudeki (1994) focused on the long duration RSTE echoes and explored their potential for neutral wind measurements. Observational and theoretical studies on RSTE and the plasma instabilities occurring within include those of Oppenheim et al. (2003), Malhotra et al. (2007), and Sugar et al. (2010). Head echoes at Jicamarca were first studied by Chau and Woodman (2004) using the interferometer mode. The abundance of meteor head echoes allows Chau et al. (2007) to determine the radiant distributions of sporadic meteors using 90 hr of observations. Gao and Mathews (2015) report meteors observed at altitudes well above 130 km.

The objective of the current report is to study meteor characteristics with a much improved sensitivity. Practically all the observations done at Jicamarca are carried out with pulse durations shorter than 65 μs. While a short length in the transmitter pulse allows the determination of meteor velocity from the elapsed range over flight time, it does not provide enough frequency resolution to make Doppler measurement without velocity aliasing. A longer pulse will provide a much better sensitivity allowing fainter meteors to be detected. The coded long pulse (CLP) technique has been frequently used at Arecibo (Li & Zhou, 2019; Sulzer, 2004). In this study, we apply the CLP technique to the Jicamarca observation. More importantly, we develop a novel probabilistic detection model that lowers the meteor detection threshold. The combination of the CLP and the probabilistic model allows us to detect a flux rate several times higher than hitherto reported. In the following, we describe our detection method after summarizing the experimental setup. We show that despite the presence of strong equatorial electrojet (EEJ), a significant amount of meteors can be still detected. After presenting the detection model, we discuss meteor characteristics that are otherwise difficult to obtain without the improved sensitivities.

Table 1
Experiment Parameters

Parameter	Value	Unit
Interpulse period	10	ms
RF pulse duration	450	μs
Transmitter baud length	1	μs
Sampling interval	1	μs
Transmitter peak power	1	MW

2. Experiment Setup

Meteor observation in this study was carried out at the JRO using the 288 × 288 m phase array on 19 September 2017. In this experiment, the JRO main phase array was divided into four equal sections (144 × 144 m). The West (W) section is used as the transmitter and North (N), East (E), and South (S) sections as receivers. The three receiver sections record complex voltage (raw data) independently and form two baselines for interferometry. The main beam is pointed 2.2° off zenith to the north to avoid EEJ contamination. Radar parameters and pulse configurations are shown in Table 1.

CLPs are generally used to improve SNR and frequency resolution while maintaining range resolution. This technique has been used very frequently at Arecibo but not often at Jicamarca (Li & Zhou, 2019; Sulzer, 2004). At the time of observation, technical difficulties prevented us from changing the transmitter pulse, a fixed 450 bits quasi-optimal code was used. This code has a maximum sidelobe of 6.7% of the main lobe. Due to transmitter duty cycle limitation, our code needs a 10 ms interpulse period, which is longer than those typically used at Jicamarca for meteor observations. Although a long interpulse period scheme may miss meteors when they travel through a pencil beam such as the Arecibo radar, JRO's main beam full-beam width at −10 dB is about 2.2°, yielding a $(3.8\ \text{km})^2$ field of view at 100 km, making it much less likely to miss meteors between pulses than at Arecibo. Figure 1 shows the antenna gain pattern. The 1 μs sampling rate allows determination of Doppler velocity ±1,500 km/s without suffering any aliasing effect. With the typical signal-to-noise ratio (SNR) at Jicamarca, Monte Carlo simulation shows that the Doppler velocity can be obtained with an accuracy of 0.3 km/s for a single pulse. Because of the high pulse compression ratio, the CLP allows detection of much weaker meteors than before.

3. Method of Meteor Detection Based on Probability

Detection of meteors is typically done by first calculating the fast Fourier transform of the raw data and then applying a SNR threshold to the power spectrum to determine the presence of a meteor (e.g., Li & Zhou, 2019). In the method described here, we use a joint probability threshold instead of SNR. In our method, we first find the power spectra of all heights of interest in every pulse. We select the largest spectral peak at every height as a potential meteor candidate. Assuming the average SNR in a power spectrum is μ, the probability density function, $f(x)$, for a random noise process to generate a spectral peak having a SNR of x is

$$f(x) = \frac{(N+1)}{\mu}\left(1-e^{-x/\mu}\right)^{N} e^{-x/\mu}, \tag{1}$$

where N is the number of data points to select the largest power from (Zhou et al., 1999). Equation (1) applies to either time or frequency domain if the N data points are independent. In many applications, however, the power spectra are zero padded from N data points to L points to improve the frequency resolution. In our case, $N = 450$, corresponding to the samples of the transmitter pulse and L is chosen to be 1,024. We are not aware of an exact theory for the probability density function shown in equation (1) in the case of zero padding. Although zero padding does not increase the number of independent points, additional sampling points in the frequency domain make the peak spectral power larger than without zero padding. The net effect is that N in equation (1) is increased. By normalizing the average SNR to 1 for convenience, we model the probability density function with zero padding as

$$f(x) \approx (N\alpha+1)\left(1-e^{-x}\right)^{N\alpha} e^{-x}, \tag{2}$$

where α is an expansion factor to account for zero padding. The value of α decreases with increasing N and approaches 1 when N approaches L. Its value can be estimated from Monte-Carlo simulations. For $N = 450$, α is found to be 2. With the probability density function given in equation (2), the cumulative probability for random noise to generate a SNR exceeding x is conveniently expressed as

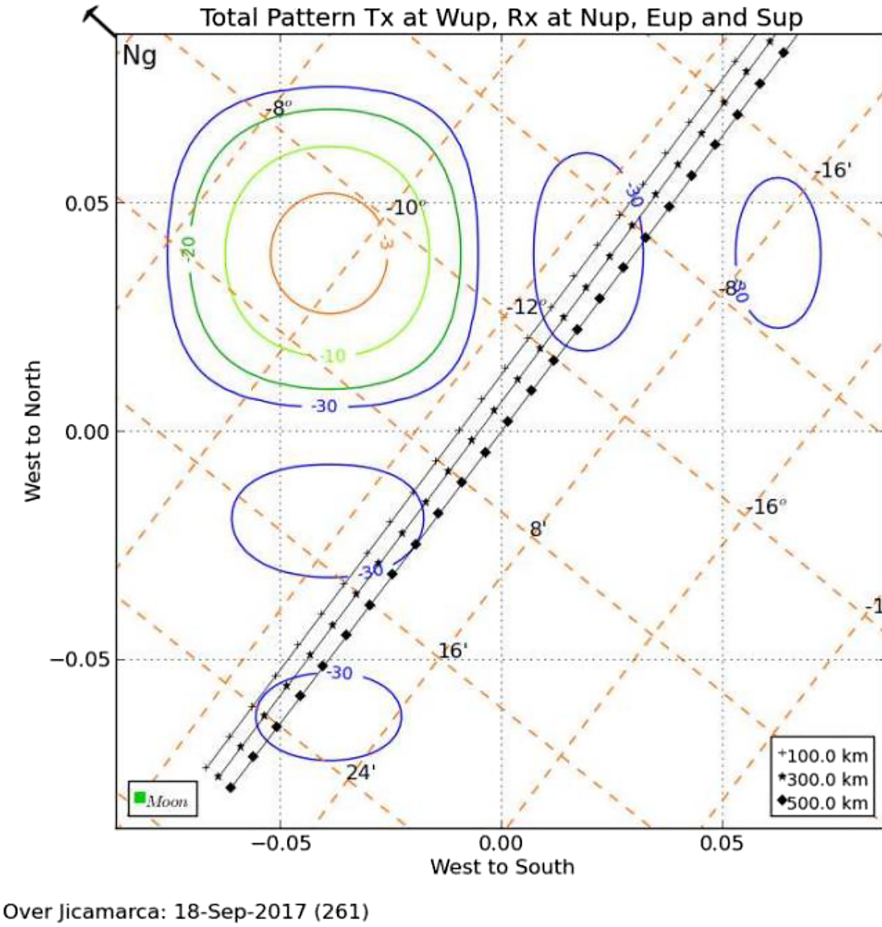

Figure 1. Antenna gain pattern for the experiment configuration.

$$F(x) = 1-(1-e^{-x})^{N\alpha} \approx N\alpha e^{-x}. \tag{3}$$

For $N\alpha = 900$, F(7.17) is 0.5, and the approximation in equation (3) has an accuracy better than 0.1% when x is larger than 10. Comparison of equations (2) and (3) with simulations and observations are shown in Figure 2, which can be seen to agree with each other very closely.

The geocentric velocity of an intrasolar meteoroid encountered by Earth is between 11 and 72 km/s, while the bandwidth of the power spectrum accommodates a much larger velocity range (±1,500 km/s). A necessary condition to associate a spectral peak to a meteor echo is for the spectral peak to fall within the frequency range corresponding to the meteoroid velocity range. Let us say that at ith pulse and jth height, the largest spectral peak has a SNR of x occurring at frequency index k. Assuming the frequency index range corresponding to the allowable velocity range be $[k_1, k_2]$, the probability that random noise generates a spectral peak larger than x within the meteor frequency range is

$$P(i,j,[k_1,k_2]) = \frac{k_2-k_1+1}{L}\left[1-\left(1-e^{-x(i,j)}\right)^{N\alpha}\right] \approx \frac{k_2-k_1+1}{L} N\alpha e^{-x(i,j)}. \tag{4}$$

If we classify a SNR of x as a meteor echo, equation (4) is the probability of false detection (PFD) for a single pulse at a single height. If the allowable meteor velocities is 5–72 km/s, the coefficient $\frac{k_2-k_1+1}{L}$ is about 2.5%. (The lower limit is smaller than the escape velocity because the velocity we use is the line-of-sight velocity.)

In meteor detection, it is important to limit the false alarm rate (FAR), defined as the number of false meteors detected per unit time, to a desirable level. The FAR is the PFD in equation (4) multiplied by the

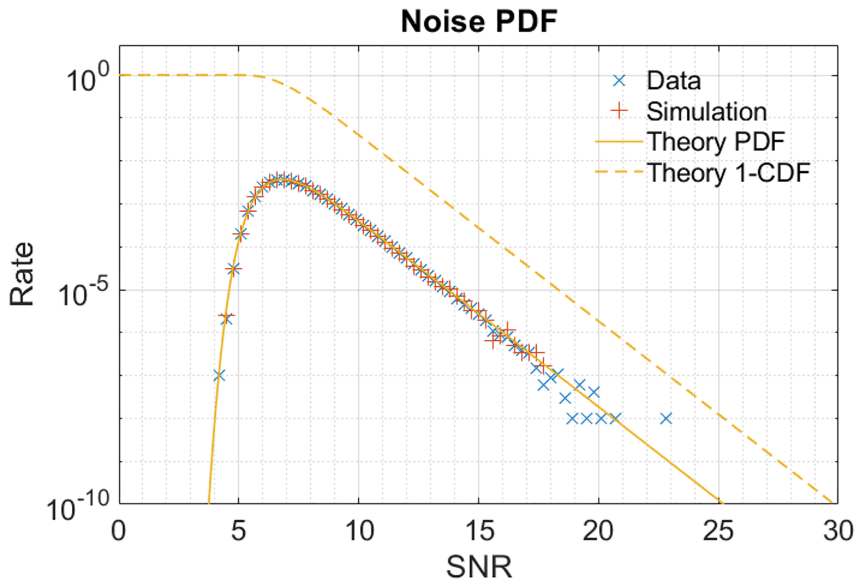

Figure 2. Comparison of probability density functions using observation data, numerical simulation, and theoretical equation. The dashed line is the theoretical complementary cumulative distribution function.

number of pulses and heights per unit time. In 1 s, we have 100 pulses and 600 height samples from 75 to 135 km. In order to have a FAR of less than 1 meteor per hour, the probability in equation (3) needs to be 10^{-7}, which corresponds to $x = 22$. If we choose a SNR threshold of 22, we may miss many meteors. In order to detect faint meteors, it is important that we consider that a meteor appears in more than one pulse. When the same meteor appears in the next pulse, the height of detection and Doppler velocity may slightly be reduced. Given that at ith pulse and jth height, the spectral peak k occurs within the allowable range; in the $(i + 1)$th pulse, we search $[j_1, j_2]$ heights to see if any spectral peaks fall around spectral peak k. This probability is equation (4) multiplied by $(j_2 - j_1 + 1)$, which is chosen to be 3. In subsequent pulses, the range of frequency is more restrictive. With both the height and frequency taken into consideration, the multiplication coefficient $\frac{k_2-k_1+1}{L}$ in equation (4) is replaced by 15/1,024. The joint PFD (JPFD) is the product of the PFD from the ith pulse and all subsequent pulses. The search process ends when a spectral peak is not found in the expected range. An event is classified as a meteor if and only if the JPFD is less than 3.85×10^{-8}. (This threshold produces an expected FAR of 8 meteors per hour for the parameters used in this study.)

After identifying an event using JPFD, an additional filter that compares the Doppler velocity with that calculated from range and time elapsed was applied to further reduce false alarms. If the two velocities differ by more than 5 km/s, the event is excluded as a meteor. This filter is effective in removing false echoes produced by the sidelobes of the transmitter code. It is only applied to echoes appearing in four or more pulses, which are needed to determine the range-time velocity to a reasonable accuracy.

Although typical meteoroid speed ranges from ~10 to 72 km/s, we choose the speed range between 5.7 and 87.9 km/s. The lower boundary is to account for the fact that the line-of-sight velocity in our observation is lower than the vector velocity. Although the line-of-sight velocity can be as low as zero, it is set to 5.7 km/s to block false alarms due to scattering from irregularities caused by EEJ. The upper boundary is set higher than 72 km/s to provide a means to estimate the FAR realistically. Echoes with a velocity faster than 72 km/s are considered as false alarms. Using the criteria mentioned above, only 17 out of 36,111 events are found to have a velocity between 72 and 88 km/s, yielding an equivalent error rate of 0.2% for velocities between 9 and 72 km/s for all meteors, or a FAR of 5 meteors per hour on average. Using a false detection probability of 3.85×10^{-8}, 100 transmitted pulses per second, and 600 detection heights per pulse, we expect 8 false meteors per hour. The lower FAR in the actual observation is due to the additional filter that compares the range-time and Doppler velocities.

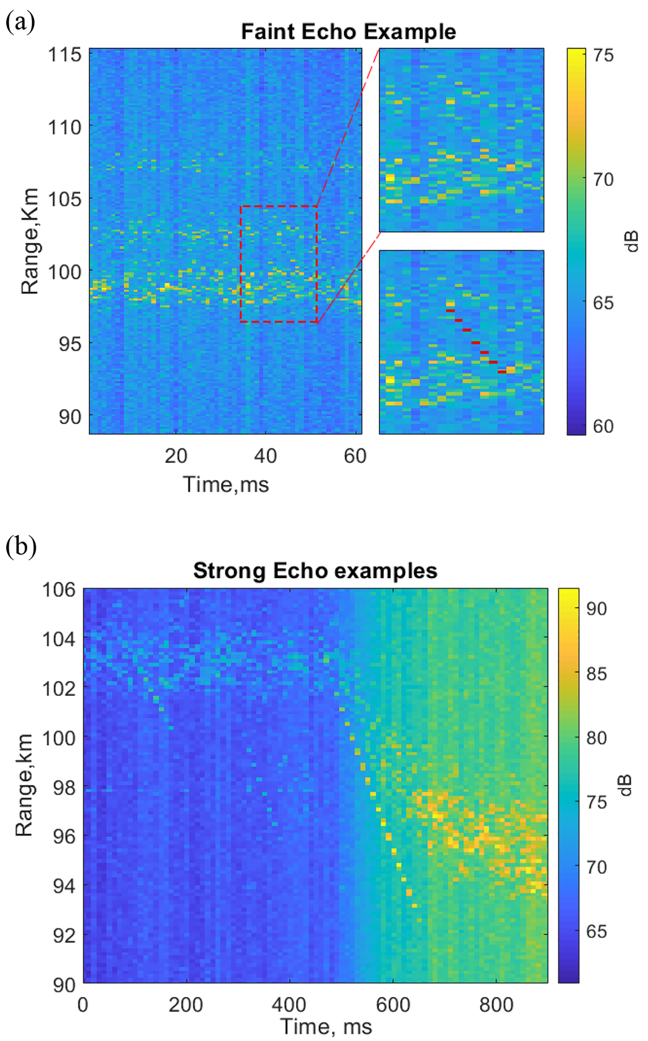

Figure 3. (a, left) Example of the largest spectral peaks as a function of pulses and heights. The strong echoes at 93 and 103 km are due to EEJ. (right up) A close up of a weak meteor head echo. (right down) The meteor echo in the upper right panel is pseudocolored as red to indicate where it is detected. (b) Examples of strong meteor head echo. Some of the strong echoes are followed by range spread trail echoes.

We are able to detect over 180 meteors per minute using the CLP and the above selection technique during the dawn hours. In comparison, Chau and Woodman (2004) report a meteor detection rate of 25 per minute with twice of our transmission power using an automated search algorithm although their rate is doubled when a manual search process is carried out (Chau et al., 2007). Figure 3 shows an example meteor echo in the presence of EEJ. Although this echo is hardly discernable from the range-time-power plot, it is readily detected by our algorithm. Statistically, the effectiveness of our method is seen from the distribution of the largest SNR for each meteor event. If the detection is based on the largest SNR, then the SNR has to be above 20 in order to have the same FAR. As seen from Figure 4, about 25% of the meteors will be missed, and most of them will be during strong EEJ. We note that the SNR in Figure 4 is based on the noise level in each pulse and each height. The noise power itself, however, varies with time and height.

4. Time and Height Distribution of Meteor Flux Rate and Velocity

Scattering from EEJ dominates the power return and presents a major problem for meteor detection at JRO because it varies strongly with time and height. For this reason, no consistent diurnal and height variations have been reported from JRO despite meteor studies have been carried out for over two decades. Figure 5 shows our meteor detection rate along with noise level, which varies according to the strength of the EEJ. The detection count is clearly anticorrelated with the noise power. Previous studies largely ignore the periods when EEJ is strong. The greater sensitivity in our approach allows the detection of a large number of meteors in the presence of very strong EEJ, such as around 1:00 a.m.

Meaningful meteor flux rate as a function of time needs to be determined at a constant noise level. As our method is sensitive enough to detect meteors even in the presence of strong EEJ, we can artificially add a noise to bring the noise to a nearly constant level. The dashed red line in Figure 5 shows the meteor detection rate when an artificially higher noise level is used. The minimum noise level we choose is 10^6 (arbitrary unit), which selects 10.9% of the meteors having the largest power. This threshold allows a constant noise power for most of the observing period. The detection rate at a constant noise power in Figure 5 is characteristic of the typical diurnal variation observed at other HPLARs (e.g., Li & Zhou, 2019; Zhou et al., 1995).

Although EEJ regions are confined to narrow layers, the noise distribution from EEJ after decoding extends to the range corresponding to the transmitter pulse, that is, 67.5 km in our case, above and below the EEJ height. This effectively evens out the noise power in altitude range. The red solid curve in Figure 6 shows the relative noise power as a function of range. The highest noise power at 100 km corresponds to the height of the strongest EEJ, while the altitude profile is largely determined by the code. The solid blue line in Figure 6 shows normalized distribution of all meteors detected without adding artificial noise, while the dotted blue curve shows the meteors detected by making the maximum noise power for all the heights in each pulse. The two curves do not differ too much statistically because the noise powers at different heights in the same pulse differ only by a factor of 2 in the most extreme case. The relative reduction in meteors detected by adding noise to those without is shown in the dashed red curve. This curve follows the trend of the background noise power. Comparison with the Arecibo height distribution (e.g., Janches et al., 2003; Zhou & Kelley, 1997) shows that the detection height at Jicamarca is noticeably higher. If we assume that meteors are mainly detected in the mainlobe, the 2.2° off zenith beam center direction can lower the

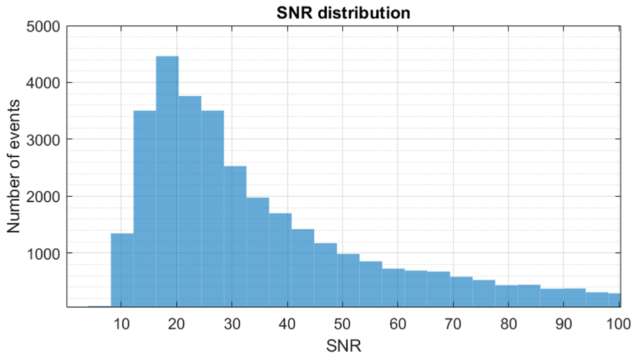

Figure 4. Meteor distribution as a function of SNR.

altitude distribution by less than 0.2 km, which is far from sufficient to account for the altitude profile difference with Arecibo. As discussed later, meteors detected by the Arecibo radar are much smaller than those detected by the Jicamarca's. For a smaller meteor to be detected by a radar, its atmospheric entry velocity needs to be larger, which ablates at a higher altitude. Thus, there is an inconsistency between the expected detection height of the Arecibo and Jicamarca meteors. One reason for this inconsistency is that a large fraction of the Jicamarca meteors is outside the mainlobe, which is discussed more quantitatively in the following.

To further explore the altitude distributions, we plot in Figure 7 the normalized detection rate as a function of range at several time intervals. As shown in Figure 6, the blue curve in each plot is for all the meteors detected without adding any artificial noise, while the dotted blue curve is for the meteors detected with a constant noise power for all the altitude. As an echo typically appears at several range gates, the range for each meteor echo is the average of the beginning and ending range. Shown in Figure 7 is also the average velocity and its standard deviation as a function of altitude for the three time intervals. Around dawn hours from 5 to 7 a.m., the large average velocity suggests that most of the meteoroids are on retrograde orbits. Meteors detected around midnight may be either on retrograde or prograde orbits, and they have a shallow atmospheric entry angle. The radiant direction is discussed in detail by Chau et al. (2007). We focus on the ablation characteristics here.

In Figure 7c, we also plot the height distribution of the Arecibo meteors using the CLP from December 2011, during which the antenna was pointed vertically (Li & Zhou, 2019). The range distributions at the two sites are very similar except that the peak range at Jicamarca is about 2 km higher than at Arecibo. The first null in the Jicamarca antenna pattern is at most 4.4°, which accounts for only 0.18 km in range-altitude difference. While there may be other factors contributing to the difference, Arecibo-Jicamarca difference can be explained by the possibility that many Jicamarca meteors are detected outside the mainlobe. The range-altitude difference of an echo 11.5° off zenith is 2 km, while the difference is 1 km at an 8° zenith angle. The center of the nth sidelobe of the Jicamarca antenna is less than $3.4 + 2.4n$ degrees off zenith by accounting for the 2.2° offset in beam center, where n is the order of the sidelobe. If a significant amount of meteors is detected at the third and fourth sidelobes, it can help to explain the difference. In fact, Vierinen et al. (2014) demonstrated that the EISCAT radar can detect meteors more than 45° off the main-beam direction. As seen in the beam pattern presented in Gao and Mathews (2015), the theoretical relative antenna gain for our configuration in the third sidelobe is −20 dB, and the actual sidelobe level can be much higher. Meteor

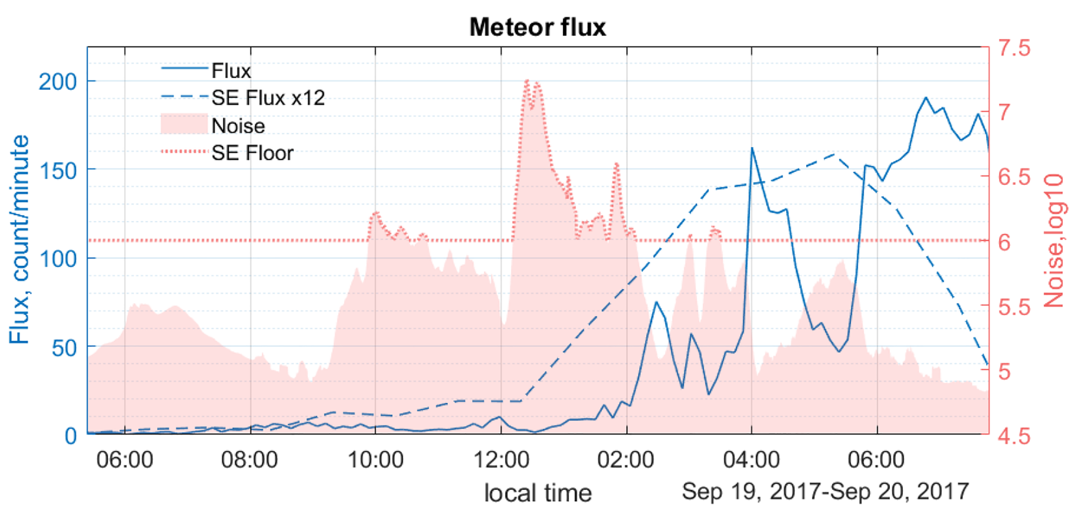

Figure 5. The solid curve is the meteor detection rate corresponding to the noise power shown by the shaded curve. The dashed blue line is the flux rate with the noise power indicated by the red dotted line, which is made constant most of the time during the observation.

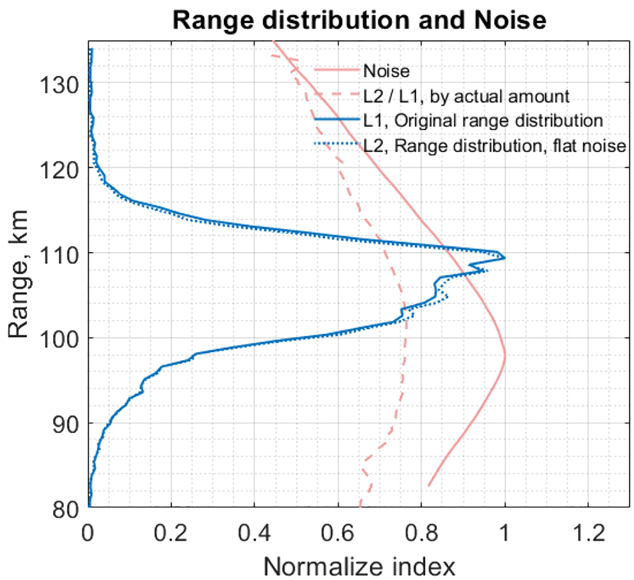

Figure 6. Distribution of normalized meteor count as a function of height. The solid blue curve uses the original noise power, while the dashed curve is for meteors with the maximum noise power found in each pulse. Solid red curve indicates the average noise power over the entire observation. The dashed red curve indicates the square of the ratio of constant noise power over the original noise power.

echoes have a very large dynamic range (more than 60 dB), and strong echoes often saturate the receiver. It should not come as a surprise that some meteors are detected in the sidelobes, what matters is at what fraction? We will discuss this further when we compare the range difference between the strong-only and the average meteor echoes.

In general, we expect meteoroids with higher velocity ablate at higher altitude as dictated by fundamental physics. As shown in Figures 7b and 7c, this is largely true from 1 to 7 a.m. and below 110 km. However, the average observed velocity above 110 km decreases with increasing altitude. Two scenarios may contribute to this characteristic: High altitude meteors may enter into the beam at a large arrival angle, and/or they may be detected in the far sidelobes of the antenna. (As the pointing direction in our experiment is nearly vertical, the arrival angle of a meteor with respect to the pointing direction is also the atmospheric entry angle.) In the first scenario, assuming a meteoroid has a velocity of 50 km/s and ablates at 110 km when it comes straight down the beam vertically. The same meteoroid will ablate at a higher altitude when it comes down with a relatively large arrival angle because the slant path effectively increases the number of collisions for the same vertical distance traversed. The effect is that a slant meteoroid will burn at a higher altitude and have a lower line-of-sight velocity than a meteoroid coming straight down the beam with the same vector velocity. In the second scenario, a meteoroid with a vertical trajectory detected close to the beam center has a larger velocity than a (vertical) meteoroid detected far from the center. As a 13° angle only reduces the line-of-sight velocity by about 2.5%, meteors picked up in the sidelobes in general do not change the average velocity significantly except for those meteors at the highest altitudes around 120 km where the

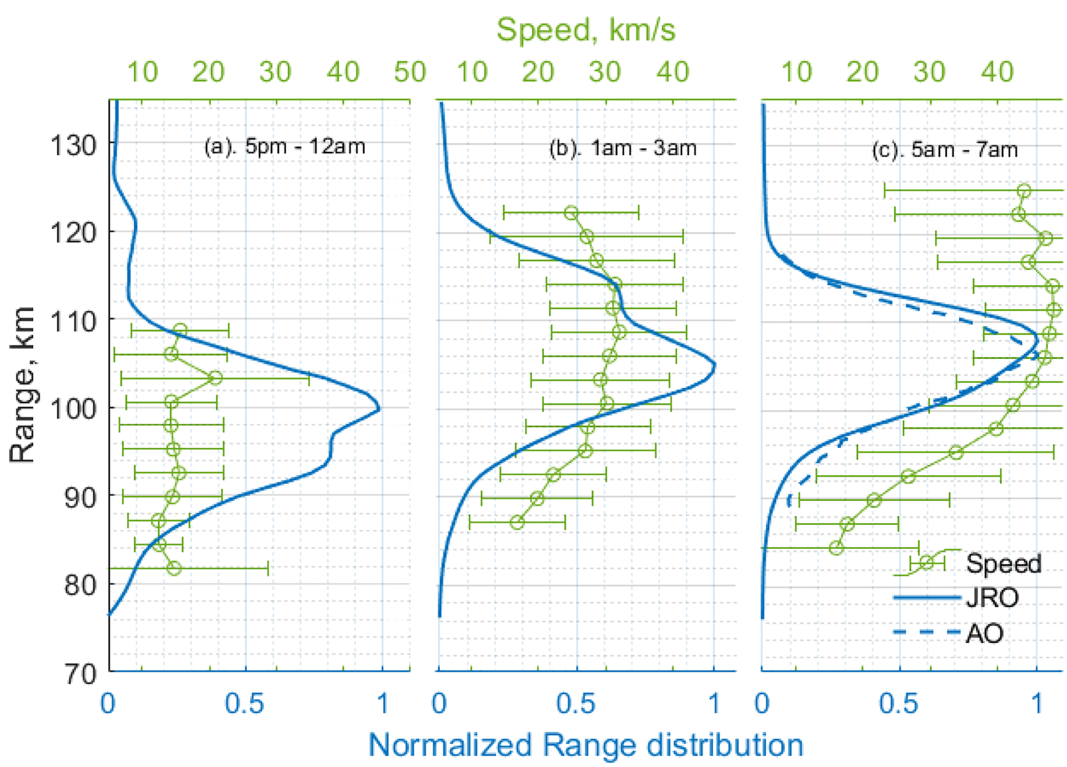

Figure 7. Normalized meteor detection rate and average velocity as a function of range for three time intervals (5 p.m. to 12 a.m., 1–3 a.m., and 5–7 a.m.). The dashed line is the range distribution at Arecibo from December 2011. The error bars indicate one standard deviation of velocity variation.

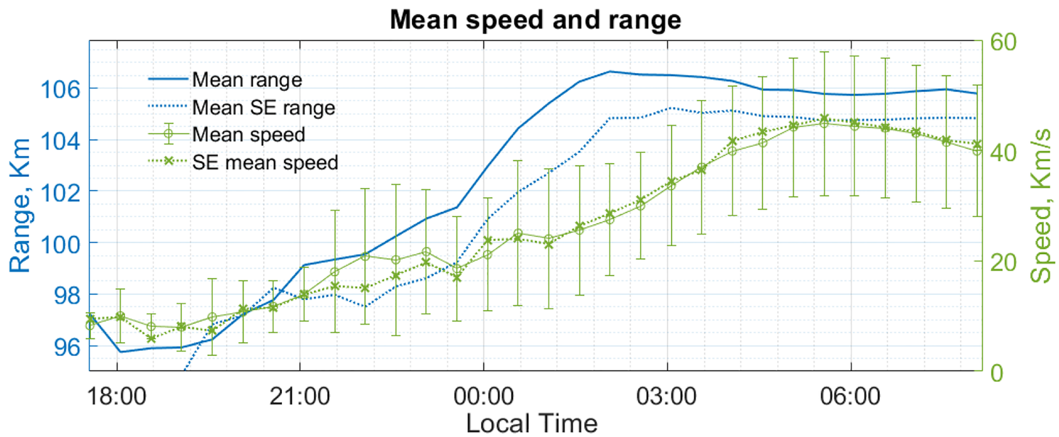

Figure 8. Average meteor echo range (blue lines) and average velocity (green lines) as a function of time. The solid curves are for all the meteors, while the dotted curves are for the top 10.7% strongest echoes.

flux rate is very low and the potential from far sidelobes is greater. Thus, while there may be a good fraction of meteors coming from the sidelobes, the fact that the highest average velocity is around 110 km is because meteors detected above this altitude have a large arrival angle.

In Figure 7a, we see the peak detection rate occurs at 100 km, and there is a flat region around 94 km. The distribution can be interpreted as the superposition of two "Gaussian" groups with their peaks at 100 and 94 km, respectively. The lower altitude group is mostly associated with meteors around 6 p.m., while the higher altitude group is mostly associated with meteors around midnight. Meteoroids detected close to 6 p.m. are on prograde orbits, and their atmospheric velocity is only slightly above the escape velocity. These meteoroids will ablate at the lowest altitude range. Around midnight, the atmospheric velocity can still be substantial, but the entry angle is small. These meteoroids will ablate at a higher altitude despite of the fact that their line-of-sight velocity is low. The slant path effect is also the reason for the "shoulder" observed at 115 km in Figure 7b. Such a "shoulder" or secondary peak effect is not in Figure 7c because dawn meteoroids have small atmospheric entry angles. A quantitative study of the ablation height on atmospheric entry angle and velocity will be done in the future using the interferometric capability of the Jicamarca radar.

The average detection height and line-of-sight velocity as a function of time are plotted in Figure 8 based on different noise threshold. The solid blue lines are for all the meteors detected, while the dashed lines are for the stronger echoes with a minimum noise power of 10^6 (i.e., corresponding to the dashed line detection rate in Figure 3). The highest average height occurs around 2:00 a.m. instead of 6 a.m. Slant path effect that accounts for the lower average velocity above 110 km in Figures 7b and 7c explains this characteristic as well. While there is hardly any difference in velocities between the two groups of meteors, the average height for the strong echoes is about 1 km lower than that for all the echoes. This characteristic is consistent with our discussion that a good fraction of Jicamarca meteors is detected in the radar sidelobes. Strong echoes tend to appear toward the beam center, while weak echoes are more likely picked up in the sidelobes. In order to account for the 1 km altitude difference, a large fraction of meteors needs to be more than 8° off the zenith angle. If we make the simplifying assumption that the number of meteors in each sidelobe deceases geometrically with increasing order of sidelobe, over 35% of the meteors will have a zenith angle larger than 8.4°. In our experimental configuration, this implies that more than 35% of the meteors are detected in the second sidelobe and beyond. If more meteors are close to the beam center, the outside meteors will need to have larger off-zenith angles to explain the altitude-range difference.

5. Discussion and Conclusion

It is of interest to compare the efficiency of the Jicamarca radar with those of other HPLARs for meteor head echo detections. Although the full main beam width is about 2°, many meteors are likely detected as far as 8° off the center. There is a large range variation of meteor mass detected by the radar with the small ones at the center and large ones in the far sidelobes. Using the entire main lobe as effective beam width (2.4°) and a detection rate of 3 meteors per second, the peak flux rate is 0.22 meteors per s/km^2 or equivalently 9×10^{14} meteors per year over the entire front side of the Earth. Using the flux rate and mass relationship found in Ceplecha et al. (1998), the Jicamarca flux rate puts the typical mass at 10^{-9} kg. In comparison, Li and Zhou (2019) report the peak flux rate at Arecibo being 10 meteors per (s•km^2) and estimate that the typical Arecibo meteor mass is at 10^{-13} kg. Based on deceleration, Mathews et al. (2001) estimated the Arecibo meteor mass range being 10^{-14}–10^{-7} kg. Close et al. (2005) reported that the mass of the meteoroids detected by the ALTAIR 166 MHZ and 422 MHZ radars is around 10^{-9} kg. Kero et al. (2008) determined that the typical mass range of the EISCAT tristatic 930 MHz is 10^{-8} kg. At the lower VHF range around 50 MHz, observations have been made by MU radar (46.5 MHz) and the Middle Atmosphere ALOMAR Radar System (53.5 MHz). These two VHF radars are slightly less sensitive than the Jicamarca radar. Kero et al. (2012) reported that 10 meteors per minute observed by the MU radar. Using deceleration, Schult et al. (2017) estimated the most prevalent mass observed by the MAASY at about $10^{-8.4}$ kg although some of the meteors may be as small as 10^{-12} kg. Other than Arecibo, the mass of the Jicamarca meteors is similar to but somewhat smaller than those observed by the VHF and UHF HPLARs.

It is generally believed that head echo is due to scattering from the overdense region, that is, where the plasma frequency exceeding the radar frequency, around the meteor head. The overdense volume at low frequency is always larger than that at high frequency. However, when the overdense region is smaller than the radar wavelength, scattering falls into the Rayleigh scattering regime, where scattered power varies with λ^{-4}. For the same overdense volume, a radar at high frequency is less affected by Rayleigh scattering than at low frequency. As the efficiency of head echo detection is largely determined by the gain of a HPLAR, this suggests that reduction to the scattering cross section in the Rayleigh regime for low-frequency radars is fairly well compensated by its larger scattering cross section. A more careful comparison of the echo rates and system parameters can yield a more quantitative description on the overdense volume at different frequency and yet insight into the evolution of plasma expansion around the head region.

To summarize, we developed a rigorous probability-based model for meteor detection. Coupled with a CLP, this method allows us to detect a large number of meteors even in the presence of strong EEJ. The detection rate of about 180 meteors per minute in the dawn hours is several times of that in previous reports. We present for the first time the meteor flux rate as a function of time and altitude with a constant noise. The average detection altitude is highest around 2:00 a.m. instead of around 6 a.m. where the largest average velocity is observed. This can be explained by the meteors at 2:00 a.m. having a larger atmospheric entry angle, which effectively increases the collision frequency per unit distance in the vertical direction. The velocity distribution during the dawn hours shows that most of the meteors are coming from relatively close to the apex direction. The maximum detection rate occurs at 98 km for dawn meteors, which is about 2 km higher than at Arecibo. More significantly, the average detection range of the strongest Jicamarca echoes is consistently 1 km above that of all echoes. If we assume the number of meteors detected in consecutive sidelobes as a geometric sequence, over 35% of the meteors will have a larger than 8° zenith angle, putting them in the second sidelobe and beyond. Meteors appearing in far sidelobes complicate some of the interpretations but need to be considered where applicable. The characteristics reported will be useful in understanding the meteoric ablation process and its relationship to radio wave scattering.

Acknowledgments
The Jicamarca Radio Observatory is a facility of the Instituto Geofisico del Peru and is operated with support from a NSF cooperative agreement through Cornell University. The study is supported by NSF Grant AGS-1744033 to Miami University. The raw data used for the analysis can be obtained from the Madrigal database at Jicamarca Radio Observatory (http://jro.igp.gob.pe/madrigal/).

References

Ceplecha, Z., Borovička, J. Í., Elford, W. G., ReVelle, D. O., Hawkes, R. L., Porubčan, V. Í., & Šimek, M. (1998). Meteor phenomena and bodies. *Space Science Reviews*, *84*(3/4), 327–471. https://doi.org/10.1023/A:1005069928850

Chapin, E., & Kudeki, E. (1994). Plasma wave excitation on meteor trails in the equatorial electrojet. *Journal of Geophysical Research*, *99*(A5), 8937–23819. https://doi.org/10.1029/93JA03198

Chau, J. L., & Woodman, R. F. (2004). Observations of meteor-head echoes using the Jicamarca 50 MHz radar in interferometer mode. *Atmospheric Chemistry and Physics (ACP)*, *4*(2), 511–521. https://doi.org/10.5194/acp-4-511-2004

Chau, J. L., Woodman, R. F., & Galindo, F. (2007). Sporadic meteor source as observed by the Jicamarca high-power large-aperture VHF radar. *Icarus*, *188*(1), 162–174. https://doi.org/10.1016/j.icarus.2006.11.006

Close, S., Oppenheim, M., Durand, D., & Dyrud, L. (2005). A new method for determining meteoroid mass from head echo data. *Journal of Geophysical Research*, *110*, A09308. https://doi.org/10.1029/2004JA010950

Gao, B., & Mathews, J. D. (2015). High-altitude meteors and meteoroid fragmentation observed at the Jicamarca Radio Observatory. *Monthly Notices of the Royal Astronomical Society*, *446*(4), 3404–3415. https://doi.org/10.1093/mnras/stu2176

Janches, D., Nolan, M. C., Meisel, D. D., Mathews, J. D., Zhou, Q. H., & Moser, D. E. (2003). On the geocentric micrometeor velocity distribution. *Journal of Geophysical Research*, *108*(A6), 1222. https://doi.org/10.1029/2002JA009789

Kero, J., Szasz, C., Nakamura, T., Meisel, D. D., Ueda, M., Fujiwara, Y., et al. (2012). The 2009–2010 MU radar head echo observation programme for sporadic and shower meteors: radiant densities and diurnal rates. *MNRAS*, *425*(1), 135–146. https://doi.org/10.1111/j.1365-2966.2012.21407.x

Kero, J., Szasz, C., Pellinen-Wannberg, A., Wannberg, G., Westman, A., & Meisel, D. D. (2008). Determination of meteoroid physical properties from tristatic radar observations. *Annales Geophysicae*, *26*(8), 2217–2228. https://doi.org/10.5194/angeo-26-2217-2008

Li, Y., & Zhou, Q. (2019). Characteristics of micrometeors observed by the Arecibo 430 MHz incoherent scatter radar. *MNRAS*, *486*(3), 3517–3523. https://doi.org/10.1093/mnras/stz1073

Malhotra, A., Mathews, J. D., & Urbina, J. (2007). Multi-static, common volume radar observations of meteors at Jicamarca. *Geophysical Research Letters*, *34*, L24103. https://doi.org/10.1029/2007GL032104

Mathews, J. D., Janches, D., Meisel, D. D., & Zhou, Q. H. (2001). The micrometeoroid mass flux into the upper atmosphere: Arecibo results and a comparison with prior estimates. *Geophysical Research Letters*, *28*(10), 1929–1932. https://doi.org/10.1029/2000GL012621

Oppenheim, M. M., Dyrud, L. P., & Ray, L. (2003). Plasma instabilities in meteor trails: Linear theory. *Journal of Geophysical Research*, *108*(A2), 1063. https://doi.org/10.1029/2002JA009548

Pellinen-Wannberg, A., & Wannberg, G. (1994). Meteor observations with eh European incoherent scatter UHF radar. *Journal of Geophysical Research*, *99*(A6), 11,379–11,390. https://doi.org/10.1029/94JA00274

Schult, C., Stober, G., Janches, D., & Chau, J. L. (2017). Results of the first continuous meteor head echo survey at polar latitudes. *Icarus*, *297*, 1–13. https://doi.org/10.1016/J.ICARUS.2017.06.019

Sugar, G., Oppenheim, M. M., Bass, E., & Chau, J. L. (2010). Nonspecular meteor trail altitude distributions and durations observed by a 50 MHz high-power radar. *Journal of Geophysical Research*, *115*, A12334. https://doi.org/10.1029/2010JA015705

Sulzer, M. (2004). Meteoroid velocity distribution derived from head echo data collected at Arecibo during regular world day observations. *Atmospheric Chemistry and Physics*, *4*(4), 947–954. SRef-ID: 1680-7324/acp/2004-4-947. https://doi.org/10.5194/acp-4-947-2004

Vierinen, J., Fentzke, J., & Miller, E. (2014). An explanation for observations of apparently high-altitude meteors. *MNRAS*, *438*(3), 2406–2412. https://doi.org/10.1093/mnras/stt2358

Zhou, Q., & Kelley, M. C. (1997). Meteor observation by the Arecibo 430 MHz ISR II. results from time-resolved observations. *Journal of Atmospheric and Solar-Terrestrial Physics*, *59*(7), 739–752. https://doi.org/10.1016/S1364-6826(96)00103-4

Zhou, Q., Tepley, C., & Suzler, M. (1995). Meteor observations by the Arecibo 430 MHz incoherent scatter radar—Results from time-integrated observations. *Journal of Atmospheric and Terrestrial Physics*, *57*(4), 421–431. https://doi.org/10.1016/0021-9169(94)E0011-B

Zhou, Q. H., Mathews, J. D., & Nakamura, T. (2001). Implications of meteor observations by the MU radar. *Geophysical Research Letters*, *28*(7), 1399–1402. https://doi.org/10.1029/2000GL012504

Zhou, Q. H., Zhou, Q. N., & Mathews, J. D. (1999). Arithmetic average, geometric average and ranking—Application to incoherent scatter radar data processing. *Radio Science*, *34*(5), 1227–1237. https://doi.org/10.1029/1999RS900062